Progress In Electromagnetics Research, PIER 64, 81–98, 2006

RESONANCE FREQUENCIES AND FAR FIELD PATTERNS OF ELLIPTICAL DIELECTRIC RESONATOR ANTENNA: ANALYTICAL APPROACH

A. Tadjalli and A. Sebak

ECE Dept, Concordia University
H3G 1M8, Montreal, QC, Canada

T. Denidni

INRS-EMT, 800 de la Gauchetiere
H5A 1K6, Montreal, QC, Canada

Abstract—In this paper the classical boundary value approach employing the separation of variable technique is used to analyze the properties of elliptic dielectric resonator antennas. In this approach, the fields inside the resonator are expanded in terms of Mathieu and modified Mathieu functions. Numerical results are given for resonant frequencies of different modes as well for fields distribution inside the resonator. Series Green's functions are used to calculate the fields inside the cavity and also far field patterns for a given feed. Using the Green's function method provides more accurate results compared to a pure cavity model technique. The analysis and design are verified through numerical simulations. A parametric study has been performed to show effects of the elliptical dielectric resonator antennas (EDRAs) parameters on far field patterns.

1. INTRODUCTION

Dielectric Resonators (DRs) have been used in many applications, such as microwave devices and antennas. Open dielectric resonators are potentially useful antenna elements [1]. They offer several attractive features such as small size, high radiation efficiency [1–3], compatibility with MIC's, intrinsic mechanical simplicity, and the ability to obtain different radiation patterns using different modes. Many of the concepts used in the design of microstrip antennas can also be used in the design of dielectric resonator antennas. Dielectric resonator

antennas have many similarities with microstrip antennas, such as small size, many possible geometries, lightweight, and ease of excitation with different excitation mechanisms. Several modes can also be excited. Each mode has different radiation characteristic. Dielectric resonator antennas have some advantages over microstrip antennas, such as wider bandwidth, higher radiation efficiency, wider range of dielectric materials, more geometrical parameters, and higher power capabilities [4].

Elliptically shaped devices are employed in many applications such as antennas, waveguides, fiber optic cables, horns and accelerator beam tubes. The elliptic structures have found increasing applications in several microwave devices, for example, microstrip antenna, dielectric resonator antenna (DRA), resonators and coaxial probe [5–9]. In particular, the elliptic geometry is becoming more popular as it allows a better control of the polarization characteristics and facilitates the design by changing both eccentricity and focal length to tune the parameters of interest. For the analysis of such devices the homogeneous Helmholtz equation in the elliptic coordinates is employed. Solving field problems of structures with elliptical geometries requires the computation of Mathieu and modified Mathieu functions [10]. These are the eigen solutions of the wave equation in elliptical coordinates.

The purpose of this paper is to present the properties of elliptical dielectric resonator antennas using analytical approach based on Mathieu functions and taking advantage of efficient numerical methods to calculate fields inside and outside the cavity. The analytical development of the solution for excitation modes and far field patterns of EDRA are presented. More accurate results are obtained by combining perfect magnetic conductor (PMC) approximation with a special Green's function to analyze EDRA. The effects of different design parameters on radiation characteristics are studied. Finally conclusions are summarized.

2. WAVE AND HELMHOLTZ EQUATION IN ELLIPTIC COORDINATES

In this section we express the three-dimensional wave equation in elliptic coordinates and investigate its solution for an elliptical dielectric resonator (EDR). The geometry of EDR is shown in Fig. 1. The EDR is mounted on a ground plane with a and b are the semi-major and semi-minor axes, respectively, and h is the height of the EDR. Image theory can be immediately applied where the ground plane is replaced by an image portion of the cylinder extending to

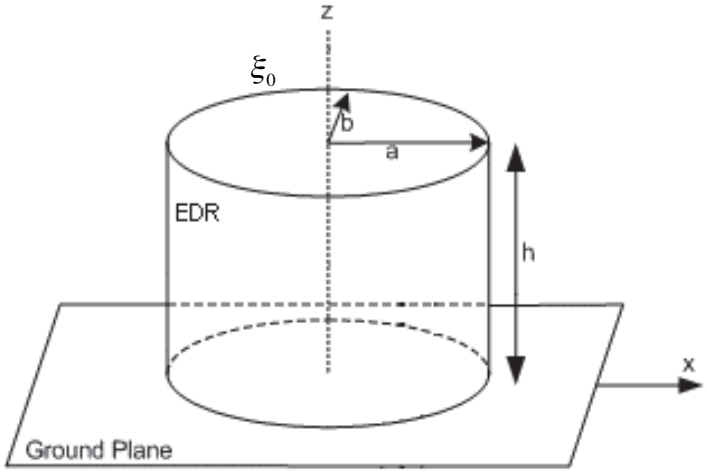

Figure 1. EDR geometry.

$z = -h$. For a DR with very large dielectric permittivity, the dielectric-air interface can be approximated by a hypothetical perfect magnetic conductor (PMC), which requires that the tangential components of the magnetic field vanish on that surface. In elliptical coordinate the scalar Helmholtz equation can be written in the form [11]:

$$\frac{2}{f_o^2\left(\cosh 2\xi - \cos 2\eta\right)}\left(\frac{\partial^2}{\partial\xi^2}+\frac{\partial^2}{\partial\eta^2}\right)\cdot\left\{\begin{array}{c} E_z \\ H_z \end{array}\right\} + (k^2 - k_z^2)\left\{\begin{array}{c} E_z \\ H_z \end{array}\right\} = 0 \tag{1}$$

Assuming that $E_z(H_z)$ can be written in the form: $R(\xi)\cdot S(\eta)\cdot \left[\begin{array}{c} \sin(k_z z) \\ \cos(k_z z) \end{array}\right]$, we can rewrite (1) as

$$\frac{1}{R}\frac{\partial^2 R}{\partial\xi^2} + \frac{k^2 - k_z^2}{2} f_o^2 \cosh 2\xi = \frac{1}{S}\frac{\partial^2 S}{\partial\eta^2} - \frac{k^2 - k_z^2}{2} f_o^2 \cos 2\eta \tag{2}$$

R and S are, respectively, the radial and angular Mathieu function, ξ is the radial coordinate, and the coordinate η is the angular coordinate. k is the wavenumber of the EDR and k_z is the wave number of the EDR in the z direction. The left- and right-hand sides of (2) must be equal to a separation constant, g. Thus (2) can be written as

$$\partial^2 S/\partial\eta^2 + (g - 2q\cos 2\eta)S = 0 \tag{3}$$

$$\partial^2 R/\partial\xi^2 - (g - 2q\cosh 2\xi)R = 0 \tag{4}$$

where

$$q \equiv \frac{k_c^2}{4} f_o^2 \tag{5}$$

$k_c = \sqrt{k^2 - k_z^2}$ is the elliptical cross-section wavenumber and f_o is semi-focal distance of ellipse. The expressions for the TE^z and TM^z modes may be written as follows: TE^z Modes:

$$\begin{aligned} H_z(\xi,\eta,z) &= \sum_{n=0}^{\infty}\sum_{m=0}^{\infty}\sum_{p=0}^{\infty}\Big\{A_{e_{nmp}}^{TE} R_{e_{nm}}^{TE}\left(q_{mn}^{TE},\xi\right) S_{e_{nm}}^{TE}\left(q_{mn}^{TE},\eta\right) \\ &\quad + A_{o_{nmp}}^{TE} R_{o_{nm}}^{TE}\left(q_{mn}^{TE},\xi\right) S_{o_{nm}}^{TE}\left(q_{mn}^{TE},\eta\right)\Big\}\sin\left(k_{z_p} z\right) \end{aligned} \tag{6}$$

TM^z Modes:

$$\begin{aligned} E_z(\xi,\eta,z) &= \sum_{n=0}^{\infty}\sum_{m=0}^{\infty}\sum_{p=0}^{\infty}\Big\{A_{e_{nmp}}^{TM} R_{e_{nm}}^{TM}\left(q_{mn}^{TM},\xi\right) S_{e_{nm}}^{TM}\left(q_{mn}^{TM},\eta\right) \\ &\quad + A_{o_{nmp}}^{TM} R_{o_{nm}}^{TM}\left(q_{mn}^{TM},\xi\right) S_{o_{nm}}^{TM}\left(q_{mn}^{TM},\eta\right)\Big\}\sin\left(k_{z_p} z\right) \end{aligned} \tag{7}$$

Where $A_{o_{nmp}}^{TE}, A_{e_{nmp}}^{TE}, A_{e_{nmp}}^{TM}$ and $A_{o_{nmp}}^{TM}$ are unknown expansion coefficients. We will use the subscript e and o to refer to even and odd modes respectively.

3. BOUNDARY CONDITIONS

For both TE and TM waves, the boundary conditions are given by:

$$H_\eta\left(\xi = \xi_0, -1 \le \eta \le 1, 0 \le z \le h\right) = 0 \tag{8a}$$
$$H_\eta\left(1 \le \xi \le \xi_0, -1 \le \eta \le 1, z = h\right) = 0 \tag{8b}$$
$$H_\xi\left(1 \le \xi \le \xi_0, -1 \le \eta \le 1, z = h\right) = 0 \tag{8c}$$
$$H_z\left(\xi = \xi_0, -1 \le \eta \le 1, 0 \le z \le h\right) = 0 \tag{8d}$$
$$E_\eta\left(1 \le \xi \le \xi_0, -1 \le \eta \le 1, z = 0\right) = 0 \tag{8e}$$
$$E_\xi\left(1 \le \xi \le \xi_0, -1 \le \eta \le 1, z = 0\right) = 0 \tag{8f}$$

where ξ_0 defines the lateral surface of the EDR. Using the boundary condition (8c) gives the resonant frequencies and can be written in the form

$$f_{\substack{e\\o}nmp}^{\binom{TE}{TM}} = \frac{c}{2\pi\varepsilon_r}\sqrt{k_{c\,\substack{e\\o}nm}^{\binom{TE}{TM}2} + k_{zp}^2} \tag{9}$$

$$\cos(k_z h) = 0 \rightarrow k_{z_p} = \frac{(2p+1)\pi}{2h}; \qquad p = 0, 1, 2, \ldots \tag{10}$$

where c is velocity of light, ε_r is the permittivity of dielectric and $k_{c\,\substack{e\\o}\,mn}^{\binom{TE}{TM}}$ is the elliptical cross-section wavenumber. The cutoff wavenumbers are obtained by setting the functions or their derivatives, depending on the boundary conditions in (8). Since fields should be single valued then the first boundary condition is given by

$$\begin{bmatrix} E \\ H \end{bmatrix}(\xi, \eta, z) = \begin{bmatrix} E \\ H \end{bmatrix}(\xi, \eta + 2\pi, z) \tag{11}$$

and the use of Mathieu function $S_{\substack{e\\o}\,nm}^{\binom{TE}{TM}}(q_{mn}^{\binom{TE}{TM}}, \eta)$ is appropriate in this case. The elliptic boundary of the membrane is given by $\xi = \xi_0$=constant, and the eccentricity e of the ellipse is defined as

$$e = \frac{f_o}{a} = \frac{1}{\cosh \xi_0} \tag{12}$$

On the elliptic boundary ($\xi = \xi_0$) the membrane is fixed, therefore

$$TE: \quad R_{\substack{e\\o}\,n}(\xi_0) = 0 \tag{13}$$

$$TM: \quad \left.\frac{\partial R_{\substack{e\\o}\,n}(\xi)}{\partial \xi}\right|_{\xi=\xi_0=0} = 0 \tag{14}$$

If we choose a certain harmonic n we have an infinite set of possible values of q that satisfy (13) and (14). Let q_{nm}^{TE} the m-th zero of R of n-order and q_{nm}^{TM} the m-th zero of derivative of R of the n-th-order. According to (8), for each q_{nm}^{TE} or each q_{nm}^{TM} there exists a corresponding frequency f_{nm}^{TE} or f_{nm}^{TM}. Solving (5) for resonant frequencies leads to

$$f_{\substack{e\\o}\,nmp}^{\binom{TE}{TM}} = \frac{c}{2\pi\varepsilon_r}\sqrt{\frac{4q_{mn}^{\binom{TE}{TM}}}{f_o^2} + k_{zp}^2} \tag{15}$$

Except for the first harmonic $n = 0$, all modes can be even or odd. Table 1 shows some resonant frequencies of an EDR and a circular cylinder dielectric resonator (CDR) with the same height and same cross section area and different e. As shown in the table, for the same range of frequency the number of resonant frequencies of EDR is more than the number of resonant frequencies of CDR with the same volume.

Table 1. Resonant frequencies of an EDR and a CDR with cross section area of $157\,\text{mm}^2$ and height of 20 mm (same volume) and permittivity of 12.

Mode	e = fo/a	Resonant Frequency (GHz)
TM110	0 (Circle)	3.748
TM111		4.840
TE010		6.051
TM210		6.494
TE011		6.781
TM112		7.547
TM211		8.046
TE012		8.144
TM113		8.260
TE013		8.809
Even TM110	0.866	3.371
Even TM210		5.188
Odd TM110		5.334
Even TE010		5.636
Odd TM210		6.756
Even TM111		6.990
Even TM310		7.132
Even TE110		7.234
Even TM211		8.026
Odd TM111		8.121
Even TE011		8.323
Odd TM310		8.339
Even TE020		8.990
Odd TM211		9.118
Even TM410		9.245
Even TM311		9.400
Even TE111		9.478
Even TM010		9.572
Odd TE110		9.684
Odd TM311		10.346

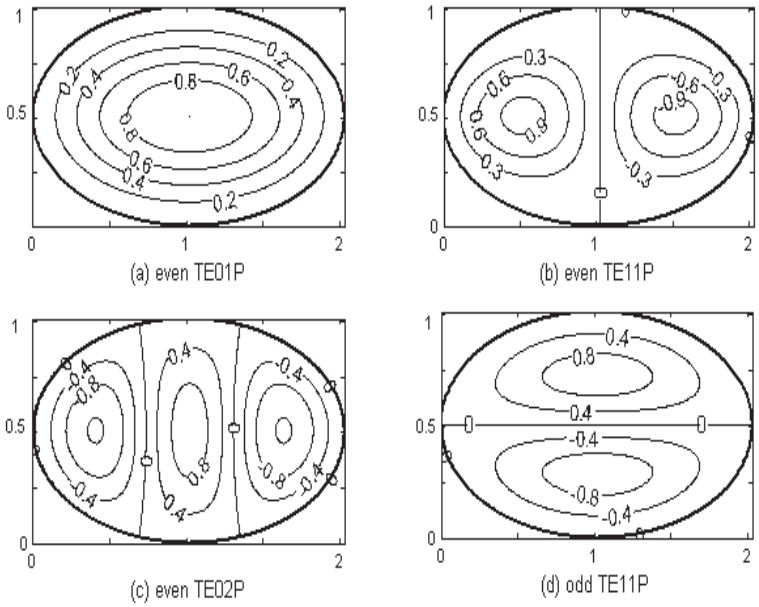

Figure 2. H_z field contour plot of TE modes.

Figs. 2 and 3 show field contours of the four lowest TM and TE modes, which are calculated using Mathieu functions. The confocal annular elliptic structure is a very versatile configuration and offers a reasonable controllability over the positions of its resonant modes. Such field's distribution patterns maybe used to determine the feed location for a special mode excitation. Mode contour patterns can also be used to recognize paths on which electric or magnetic fields are zero. This allows the study of different EDR portions for different modes. For example, in Fig. 2(c) there are 2 paths with $H_z = 0$ with 3 portions of EDR for even $\mathrm{TE}_{02\mathrm{P}}$ mode.

4. FAR FIELD PATTERN

The radiation patterns of the EDRA, shown in Fig. 4, are calculated using a two-step process.

4.1. Current Distribution on the Probe

In the first step the electric field integral equation for the current distribution on the probe's equivalent wire ($2l$) is formulated in terms

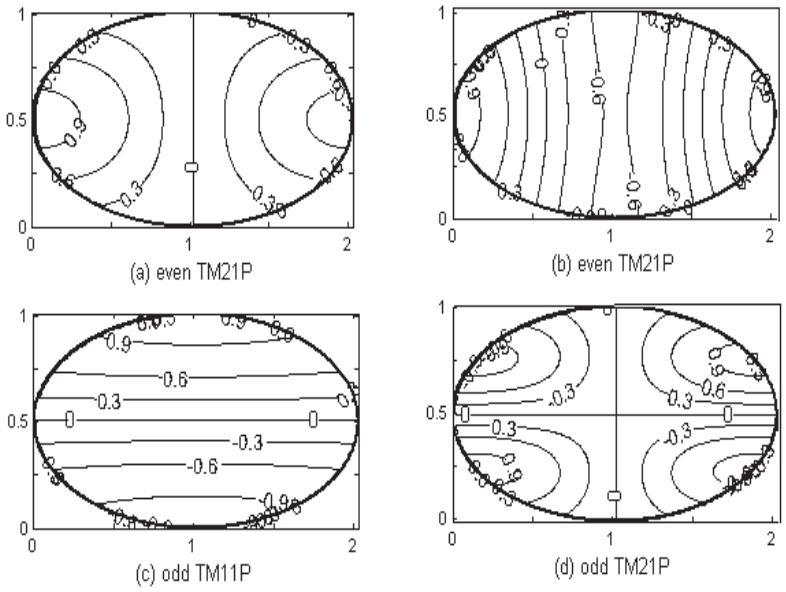

Figure 3. E_z Field contour plot of TM modes.

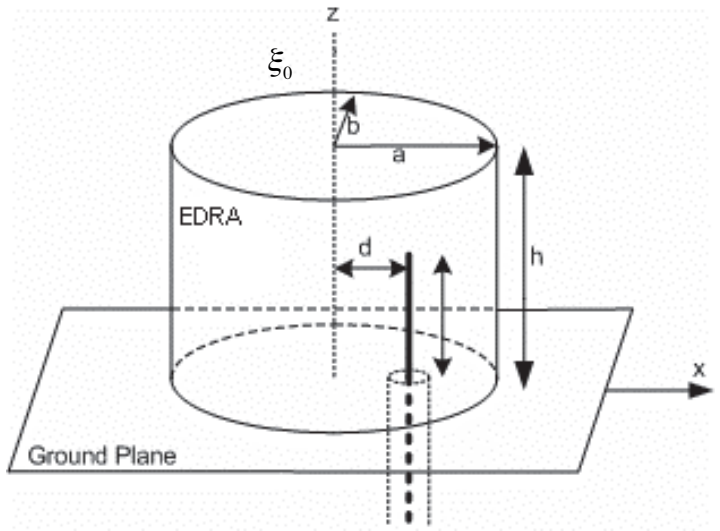

Figure 4. EDRA geometry and feed Configuration.

of the specialized Green's functions. The integral equation is then solved using the method of moments with piecewise sinusoidal bases and testing functions. The moment method is applied to calculate the current distribution on the probe. Since the eigen-functions of the media are known, the series form Green's function can be used. The eigen-function of elliptical cylinder dielectric resonator can be expressed in the form:

$$\psi_{\substack{e\\o}nmp}^{\binom{TE}{TM}}\left(q_{mn}^{\binom{TE}{TM}},\xi,\eta,z\right) = R_{\substack{e\\o}nm}^{\binom{TE}{TM}}\left(q_{mn}^{\binom{TE}{TM}},\xi\right) S_{\substack{e\\o}nmp}^{\binom{TE}{TM}}\left(q_{mn}^{\binom{TE}{TM}},\eta\right)\cos(k_{zp}z) \quad (16)$$

Thus the Green's function of the EDR can be represented as a series of eigen functions:

$$G(\xi,\eta,z,\xi',\eta',z') = \sum_{m=0}^{\infty}\sum_{n=1}^{\infty}\sum_{p=0}^{\infty}\frac{\psi_{\substack{e\\o}nmp}^{\binom{TE}{TM}}\left(q_{mn}^{\binom{TE}{TM}},\xi,\eta,z\right)\psi_{\substack{e\\o}nmp}^{\binom{TE}{TM}}\left(q_{mn}^{\binom{TE}{TM}},\xi',\eta',z'\right)}{T_{\substack{e\\o}mnp}^{\binom{TE}{TM}}\left(k^2-k_{zp}^2-k_{c\,\substack{e\\o}nmp}^{\binom{TE}{TM}2}\right)} \quad (17)$$

T_{mn} is a normalization factor.

$$T_{\substack{e\\o}mnp}^{\binom{TE}{TM}} = \int_1^{\xi_0}\int_0^{2\pi}\int_{-h}^{h}\psi_{\substack{e\\o}nmp}^{\binom{TE}{TM}2}\left(q_{mn}^{\binom{TE}{TM}},\xi,\eta,z\right)\left[\cosh 2\xi-\cos 2\eta\right]dzd\eta d\xi \quad (18)$$

To calculate the probe current distribution, the magnetic frill generator is applied as a source and piecewise sinusoids subdomain functions are used as the basis functions.

4.2. Calculations of the Radiated Field

In the second step, once the current distribution on the probe is computed, the magnetic vector potential inside the cavity can be

derived easily in the form:

$$A_z(\xi,\eta,z) = \sum_{m=0}^{\infty}\sum_{n=1}^{\infty}\sum_{p=0}^{\infty}\int_{-l}^{l} I(\xi',\eta',z')G(\xi',\eta',z',\xi,\eta,z)dz' \qquad (19)$$

Using the magnetic vector potential, the electric and magnetic fields can be computed everywhere inside the EDR. The surface magnetic current on the cavity walls is defined as

$$\vec{M} = \vec{E} \times \hat{n} \qquad (20)$$

where $\hat{n}$ is a unit normal pointing out of the dielectric. The electric vector potential is then expressed as

$$\vec{F} = \frac{\varepsilon_0}{4\pi}\iint_s \vec{M}_s(r')\frac{e^{-jk_0R}}{R}ds' \qquad (21)$$

where R represents the distance from any point on the EDR surface to the observation point. The far electric field components are obtained using:

$$E_\varphi = +j\omega F_\theta \qquad (22)$$

$$E_\theta = -j\omega F_\varphi \qquad (23)$$

5. NUMERICAL RESULTS

Results for the far field patterns, based on our developed technique and those obtained using Ansoft HFSS [12] program, are shown in Figs. 5 and 6. The results are computed at two resonance frequencies of an elliptical DRA with $a = 15\,\text{mm}$, $b = 11.25\,\text{mm}$, $h = 16.5\,\text{mm}$, relative permittivity of 9.8, $d = 7.5\,\text{mm}$ and $l = 7\,\text{mm}$. In general, good agreement is noticed between the present method and simulation results except for the cross polarization results.

Next, a parametric study has been conducted to determine the influence of various design parameters on directivity patterns of EDRAs. Due to a large number of possible combinations, only selected values are considered for this study. For the fixed probe position on the x-axis and at 4 mm from the center, Fig. 7 shows the directivity patterns in $\varphi = 0$ and $\varphi = 90$ planes for different elliptic axial ratios. By changing the axial ratio of the ellipse, excited modes change and therefore far field pattern and its nulls can be controlled by controlling the axial ratio. The influence of the EDRA height (h) on

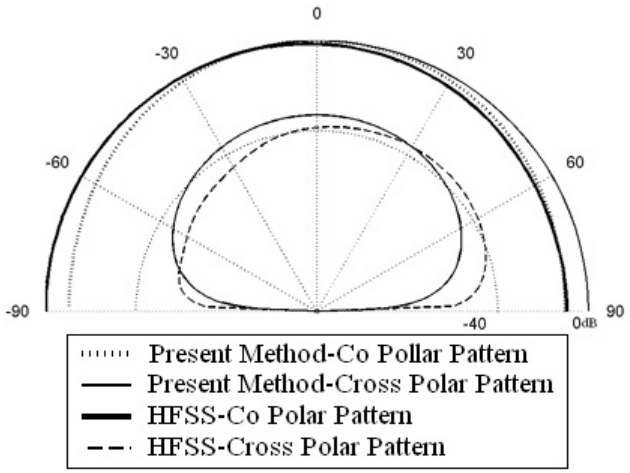

(a)

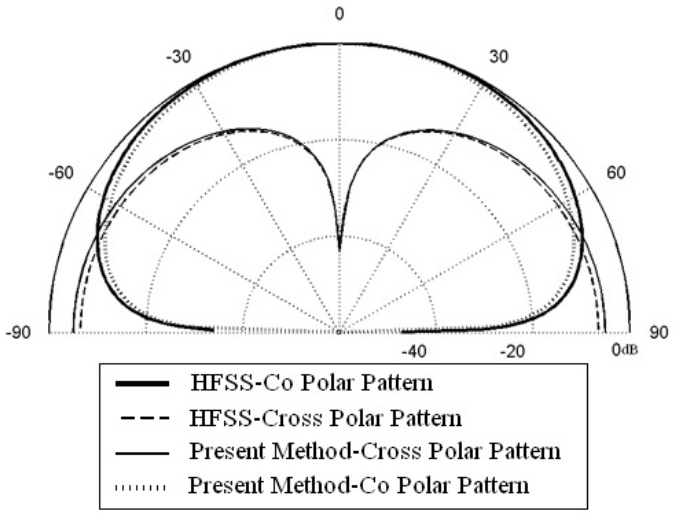

(b)

Figure 5. Radiation Patterns at frequency 3.04 GHz (a) $\varphi = 0$, (b) $\varphi = 90$, $a = 15\,\text{mm}$, $b = 11.25\,\text{mm}$, $h = 16.5\,\text{mm}$, $\varepsilon_r = 9.8$, $d = 7.5\,\text{mm}$, $l = 7\,\text{mm}$.

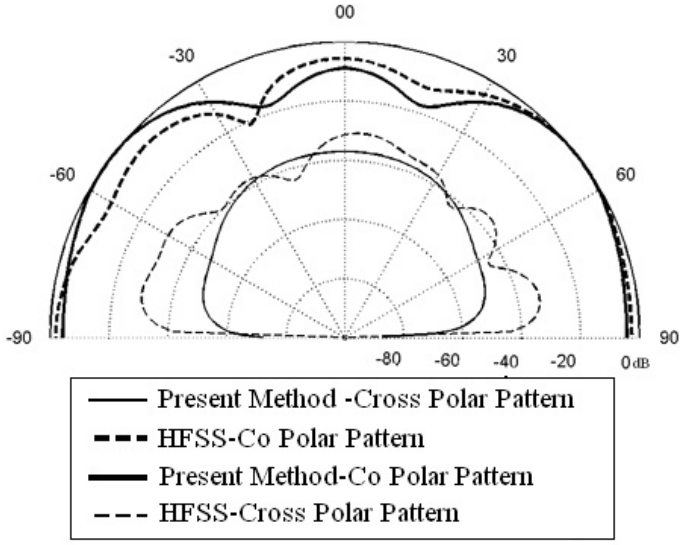

(a)

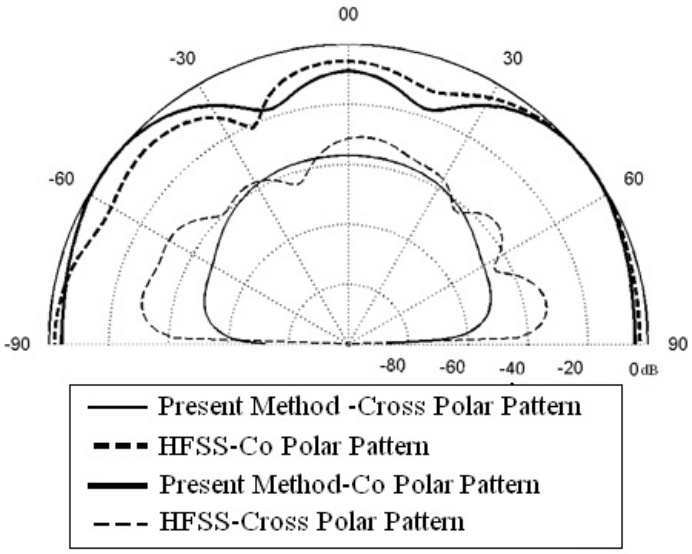

(b)

Figure 6. Radiation Patterns at frequency 7.41 GHz (a) $\varphi = 0$, (b) $\varphi = 90$ $a = 15\,\text{mm}$, $b = 11.25\,\text{mm}$, $h = 16.5\,\text{mm}$, $\varepsilon_r = 9.8$, $d = 7.5\,\text{mm}$, $l = 7\,\text{mm}$.

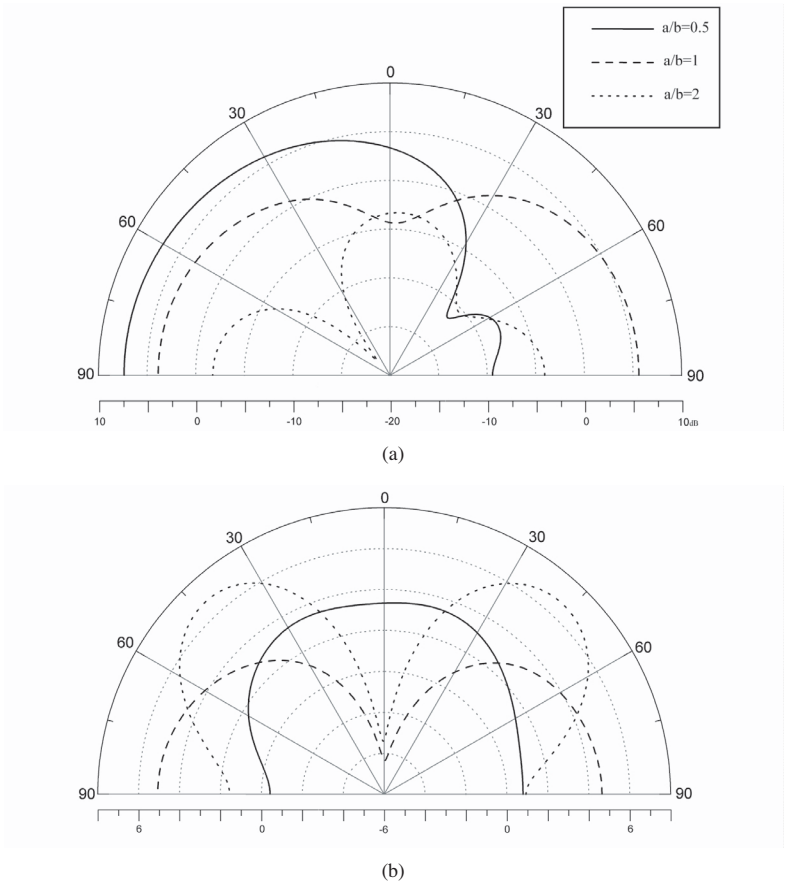

Figure 7. Far field pattern of EDRAs with $h = 7\,\text{mm}$, $d = a/2$ and $\varepsilon_r = 12$ at frequency 5.8 GHz (a) $\varphi = 0$, (b) $\varphi = 90$.

the beamwidth can be clearly seen in Fig. 8. For different heights, the radiation pattern in $\varphi = 0$ plane does not have a noticeable change but in $\varphi = 90^\circ$ we can see variations in the beamwidth with h. Increasing the height does not change the elliptic cross-section exited modes. It only affects the z direction modes. Fig. 9 shows the calculated directivity patterns for identically sized cylinders with different values of the dielectric constant. Effect of increasing permittivity is similar to increasing the equivalent electric volume of EDRA. Another important design parameter is the position of the probe inside the EDRA. Fig. 10 shows the directivity patterns for different positions of probe. With different locations of probe we can control excitation of special modes.

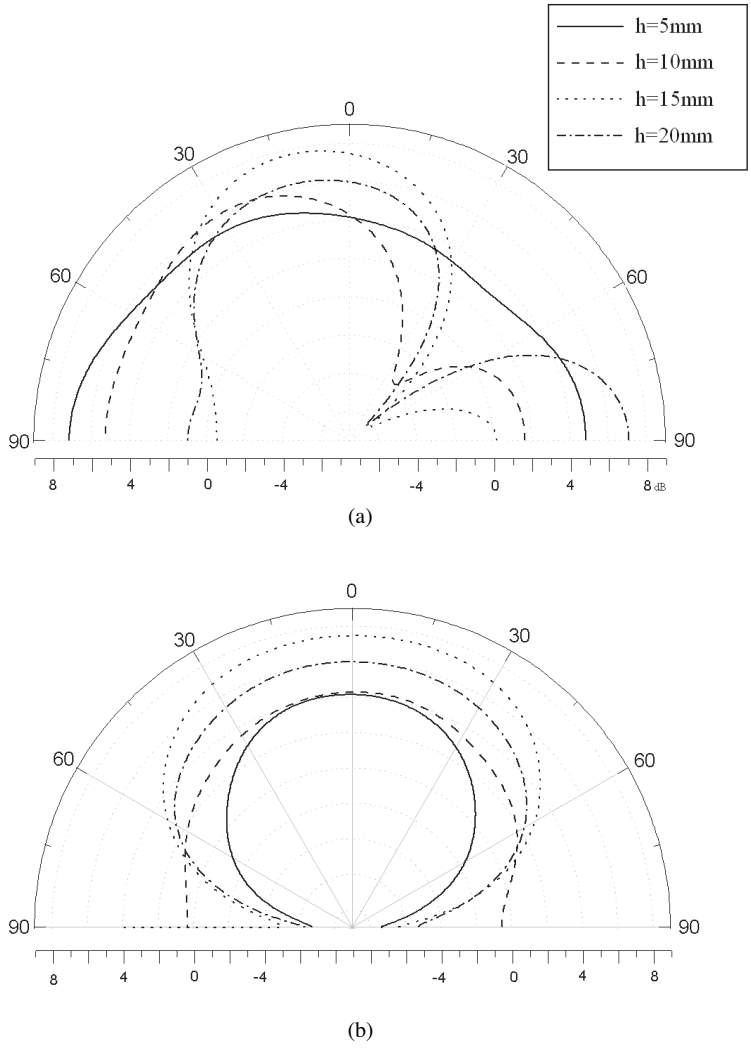

Figure 8. Far field pattern of EDRAs with $a = 10\,\text{mm}$, $a/b = 2$, $d = 4\,\text{mm}$ and $\varepsilon_r = 12$ at frequency $5.8\,\text{GHz}$ (a) $\varphi = 0$, (b) $\varphi = 90$.

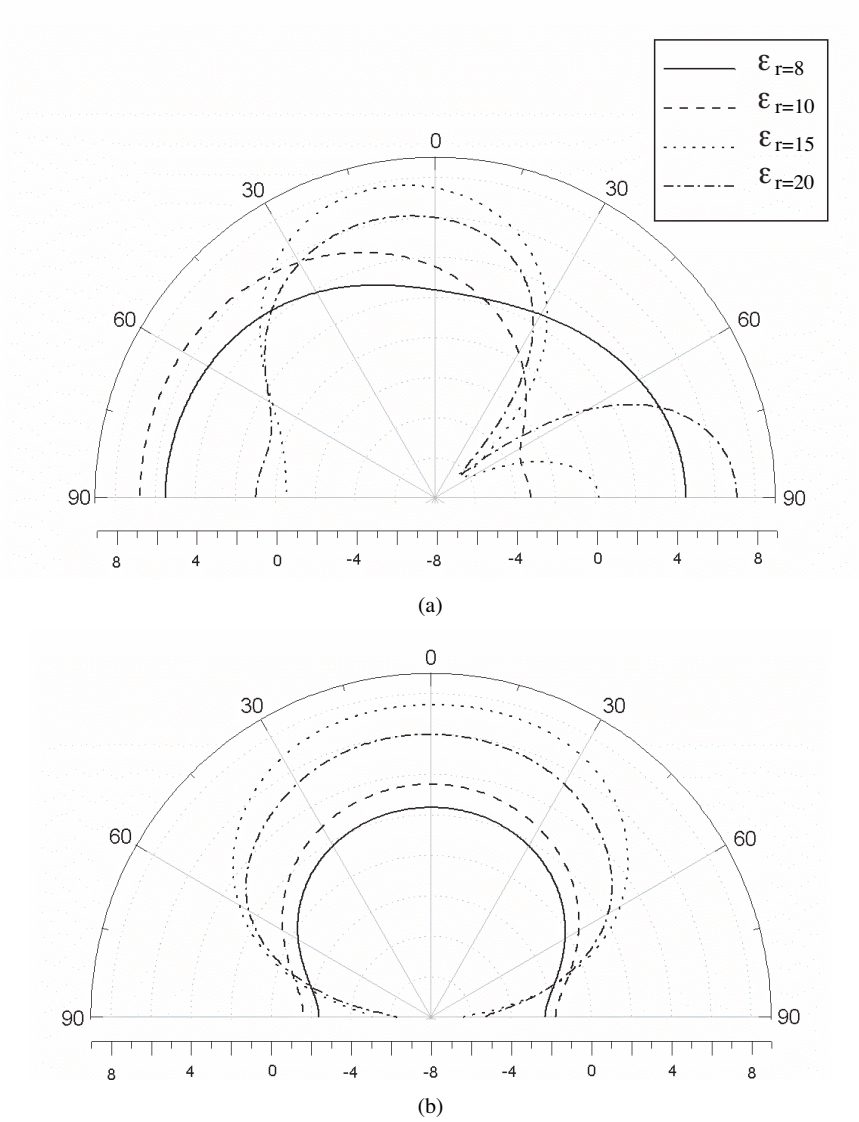

Figure 9. Far field pattern of EDRAs with $a = 10\,\text{mm}$, $a/b = 2$, $d = 4\,\text{mm}$ and $h = 7\,\text{mm}$ at frequency 5.8 GHz (a) $\varphi = 0$, (b) $\varphi = 90$.

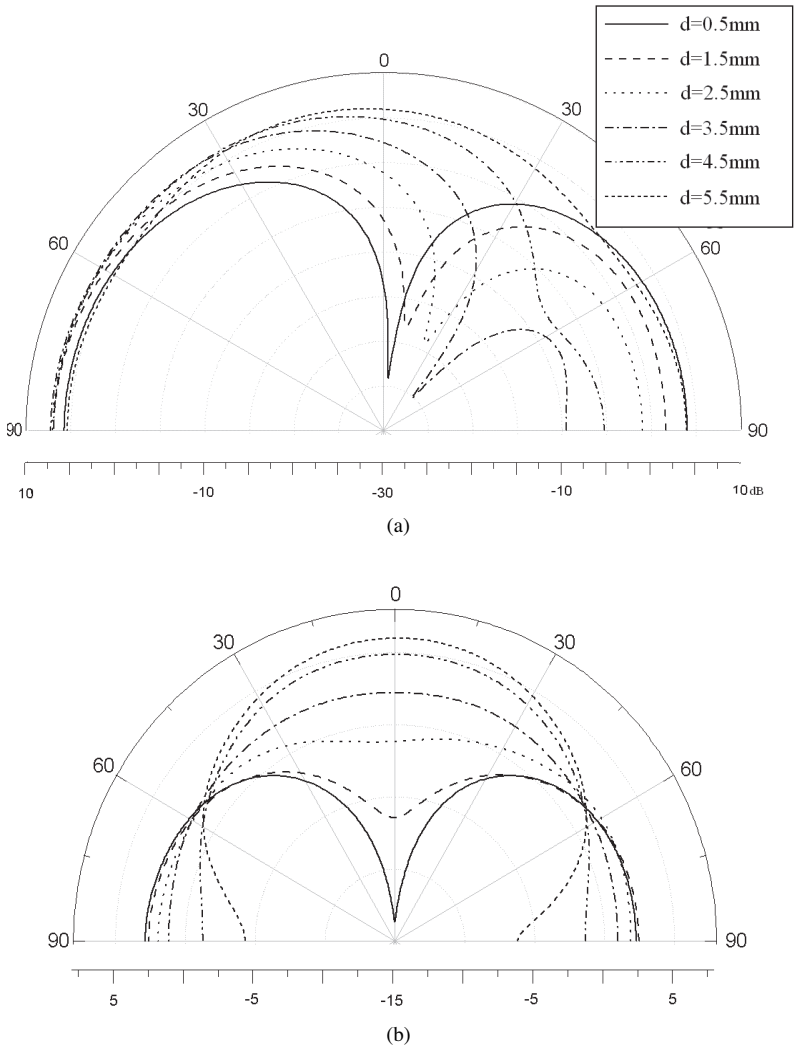

Figure 10. Far field pattern of EDRAs with $a = 10\,\text{mm}$, $a/b = 2$, $h = 7\,\text{mm}$ and $\varepsilon_r = 12$ at frequency 5.8 GHz (a) $\varphi = 0$, (b) $\varphi = 90$.

6. CONCLUSION

In this paper we presented the solution of the wave equation in elliptic coordinates including the characteristic frequencies and mode equation in EDRs. The excitation modes can be expressed in terms of a linear combination of Mathieu functions. The modes and resonant frequencies of propagation of EDRAs have been investigated theoretically in this paper. The mode-matching method has been used to derive the characteristic equation of the antenna configuration, and the source-free resonant modes and frequencies are computed. To study the radiation characteristics of the EDRA, the Green's function for the structure is derived and presented. The current distribution on the probe has been found using the MoM. The concepts presented here are general enough and enable us to recognize different excitation modes and their corresponding radiation patterns which are not possible using CAD tools. Numerical results are presented for several modes, and some calculated resonance frequencies of a sample EDR are shown. Numerical results are also presented for several configurations to show the dependence of the directivity patterns on various design parameters.

REFERENCES

1. Mongia, R. K. and P. Bhartia, "Dielectric resonator antennas — A review and general design relations for resonant frequency and bandwidth," *Int. J. Microwave Millimeter-Wave Eng.,* Vol. 4, 230–247, July 1994.
2. Mongia, R. K., A. Ittipiboon, and M. Cuhaci, "Measurement of radiation efficiency of dielectric resonator antennas," *IEEE Microwave Guided Wave Lett.,* Vol. 4, 80–82, Mar. 1994.
3. Petosa, A., A. Ittipiboon, Y. M. M. Antar, D. Roscoe, and M. Cuhaci, "Recent advances in dielectric resonator antenna echnology," *IEEE Antennas Propagat. Mag.,* Vol. 40, 35–48, June 1998.
4. Kishk, A., "Application of rotated sequential feeding for circular polarization bandwidth enhancement of planar arrays with single-fed DRA elements," *IEEE Antennas and Propagation Society International Symposium,* Vol. 4, 664–667, June 2003.
5. Bhattacharyya, A. K. and L. Shafai, "Theoretical and experimental investigation of the elliptical annual ring antenna," *IEEE Trans. Antennas Propagat.,* Vol. AP-36, No. 11, 1526–1530, Nov. 1988.

6. Hu, Y., F. M. Ghonnouchi, and R. G. Bosisio, "Theoretical and experimental measurement of microwave permittivity using open ended elliptical coaxial probes," *IEEE Trans. Microwave Theory Tech.,* Vol. MTT-40, 143–150, Jan. 1992.
7. Sun, K. and J. M. Tranquilla, "Study of elliptical annular microstrip antenna using full Mathieu formulation," *IEEE Intern. Symp. on Antennas and Propagat.,* Vol. AP-S-2, 944–947, 1994.
8. Alhargan, F. A. and S. R. Judah, "Wide-band confocal annular elliptic microstrip antenna," *IEEE Int. Sym. on Antennas and Propagat.,* Vol. AP-S-2, 1006–1009, 1995.
9. Tadjalli, A. and A. R. Sebak, "Elliptical cylinder dielectric resonator antenna," *Antem International Symposium,* Ottawa, August 2004.
10. Morse and H. Feshbach, *Methods of Theoretical Physics,* McGraw-Hill, Inc., New York, NY, 1953.
11. Holland, R. and V. P. Cable, "Mathieu functions and their applications to scattering by a coated strip," *IEEE Trans. Electromagnetic Compatibility,* Vol. 34, No. 1, Feb. 1992.
12. Ansoft High Frequency Structures Simulator (HFSS), Version 9.0: Ansoft Corporate.